CrossMark

ORIGINAL ARTICLE

A software solution to dynamically reduce metallic distortions of electromagnetic tracking systems for image-guided surgery

Mengfei Li[1,2] · **Christian Hansen**[2] · **Georg Rose**[1]

Abstract

Purpose Electromagnetic tracking systems (EMTS) have achieved a high level of acceptance in clinical settings, e.g., to support tracking of medical instruments in image-guided interventions. However, tracking errors caused by movable metallic medical instruments and electronic devices are a critical problem which prevents the wider application of EMTS for clinical applications.

Methods We plan to introduce a method to dynamically reduce tracking errors caused by metallic objects in proximity to the magnetic sensor coil of the EMTS. We propose a method using ramp waveform excitation based on modeling the conductive distorter as a resistance-inductance circuit. Additionally, a fast data acquisition method is presented to speed up the refresh rate.

Results With the current approach, the sensor's positioning mean error is estimated to be 3.4, 1.3 and 0.7 mm, corresponding to a distance between the sensor and center of the transmitter coils' array of up to 200, 150 and 100 mm, respectively. The sensor pose error caused by different medical instruments placed in proximity was reduced by the proposed method to a level lower than 0.5 mm in position and 0.8° in orientation. By applying the newly developed fast data acquisition method, we achieved a system refresh rate up to approximately 12.7 frames per second.

Conclusions Our software-based approach can be integrated into existing medical EMTS seamlessly with no change in hardware. It improves the tracking accuracy of clinical EMTS when there is a metallic object placed near the sensor coil and has the potential to improve the safety and outcome of image-guided interventions.

Keywords Electromagnetic tracking · Image-guided interventions · Clinical navigation systems · Error reduction · Metallic distortion

✉ Mengfei Li
  Mengfei.li@ovgu.de

1 Chair for Medical Telematics and Medical Technology, Institute of Medical Technology, Otto-von Guericke Universität Magdeburg, G09-324, Universitätsplatz 2, 39016 Magdeburg, Germany

2 Research Group of Computer-Assisted Surgery, Institute of Simulation and Graphics, Otto-von-Guericke Universität Magdeburg, G29-209, Universitätsplatz 2, 39016 Magdeburg, Germany

Introduction

In recent years, tracking systems have been proposed to assist image-guided interventions. The requirements for high accuracy and a fast update rate lead to an extensive use of optical tracking systems (OTS) and EMTS. While line-of-sight problems limit the application of OTS, EMTS allow the free tracking of magnetic sensors integrated into the surgical instruments' tips [1]. EMTS have been studied to be compatible in CT-guided [2] and ultrasound (US-) guided [3] interventions. However, distortions caused by metallic objects in the clinical environment cause unacceptable tracking errors. The distortions from the metallic structure of a dental drill body in dental implant surgery [4], the metallic arm support in interstitial brachytherapy treatments [5] and electronic devices such as ultrasound scanner probes in operating room (OR) [6] causes inaccuracy in sensor pose estimation. This problem prevents EMTS from being more widely utilized [7].

The two primary classifications of metallic distortions of EMTS are ferromagnetic and conductive distortions. The magnetic flux density of the material can be presented as an equation considering the magnetization:

Springer

$$B = \mu_0 (1 + \chi) H = B_0 + \mu_0 \chi H \qquad (1)$$

Here, B is the magnetic flux density, and B_0 is the reference magnetic field outside of the metal, H is the magnetic field strength, μ_0 is the magnetic permeability of vacuum and χ is the magnetic susceptibility [8]. For paramagnetic and diamagnetic materials, the magnetic susceptibility χ is linear while it is nonlinear for ferromagnetic materials. Due to the magnetic hysteresis effect [9], it is difficult to analytically categorize the secondary magnetic field generated by the ferromagnetic object. Commonly applied medical instruments, such as hammers and needles, are usually made of non-ferromagnetic materials such as aluminum and stainless steel. This work focuses on reducing distortions caused by materials that are conductive but non-ferromagnetic.

Placing sources of distorters at a sufficient distance from the EMTS can minimize the level of tracking errors [10]. Existing calibration algorithms based on correcting the errors between multiple actual and measured tracker positions [11] run offline to compensate for the stationary metal distortions. A novel method [12] using an extra sensor coil as the reference with fixed location to the tracker coil is a promising option for online calibration. Shielding methods of using shielded coils [13] or side shields to the metallic distorters [14] were put forward in patents. Pulsed direct current (DC) EMTS reduce distortions caused by eddy currents. However, such systems work slowly and are influenced by the earth's electromagnetic field [15]. By operating EMTS at the very

low frequency, the strength of the eddy currents decreases to a low level; this, in turn, reduces the interference from distorters [16]. Nevertheless, at such a low frequency, the sensor coil measures the voltage with an ultra-low signal-to-noise ratio (SNR) that often causes an inaccurate sensor pose estimation. A method for dynamically adjusting the eddy current distortions was referred in the patent [17]. However, to achieve this, a plurality of sensing elements is needed.

The input signals of an alternating current (AC) EMTS are commonly sine-wave shaped [18]. In our previous research, a method to reduce eddy current distortions by using quadratic-rectangular (QR) excitations was developed. The main drawback of the method is the slow refresh rate—approximately 1.6 fps [19].

Materials and methods

Experimental setup

Many groups use commercial EMTS for their clinical research. However, they allow no hardware or software changes to the underlying technology. We developed an EMTS experimental setup addressing flexibility, high precision, and speed (Fig. 1).

The field programmable gate array (FPGA) inside the data acquisition (DAQ) board (PXIe 7854R, National Instrument, USA) generates the waveform signals through its digital to analog converter (DAC). The generated voltage signals were
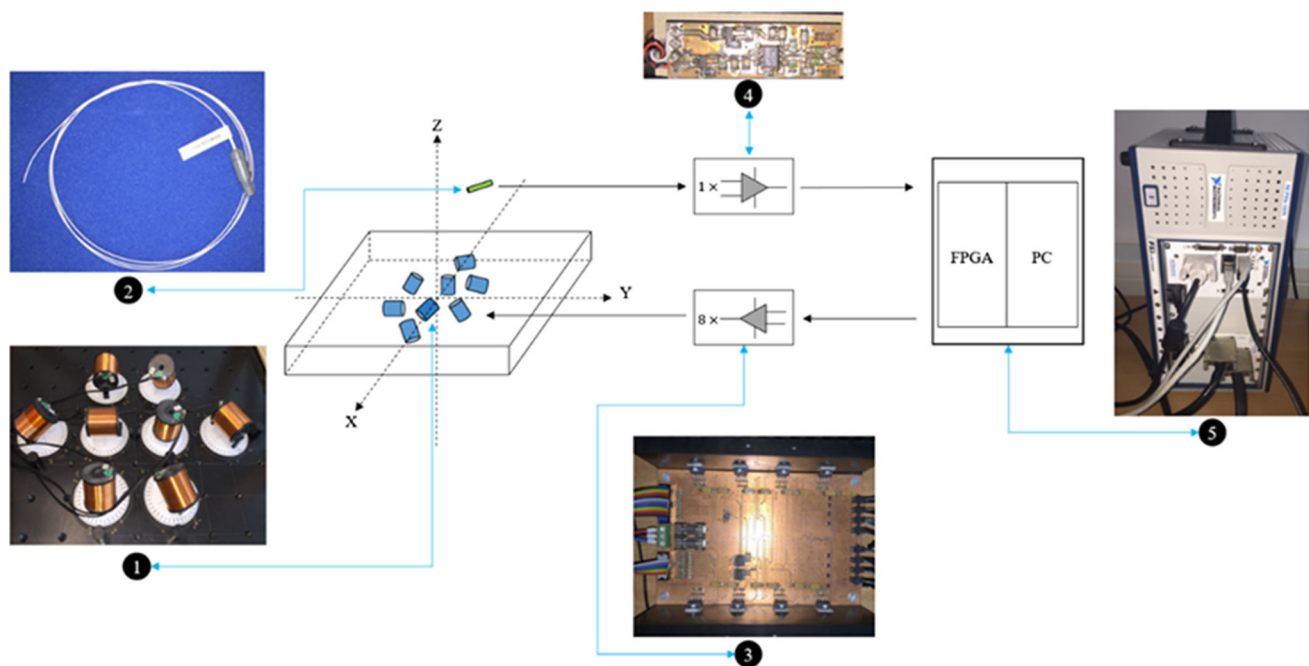

Fig. 1 Schematic diagram of our ETMS configuration: *1* eight self-developed transmitter coils, *2* sensor coil, *3* eight current-feedback amplifiers for signal generation, *4* pre-amplifier for the measured signals, and *5* the control and signal generation and data acquisition system comprising an FPGA and a PC
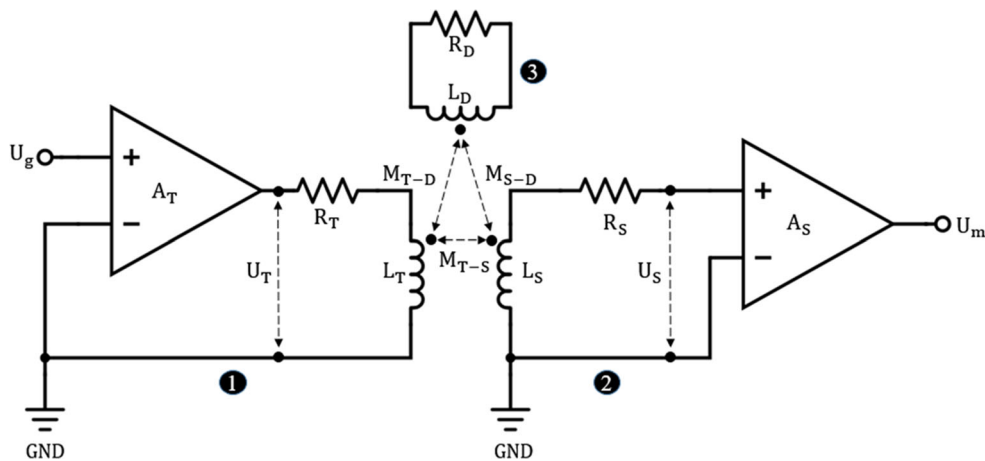
Fig. 2 The RL circuit model of *1* one out of the eight transmitter coil circuits, *2* the sensor coil circuit and *3* the circuit of the conductive distorter

driven by eight current-feedback amplifiers (LT1210, Linear Technology, USA) and sent to the transmitter coils to produce magnetic fields. A magnetic sensor coil (NDI 5-DOF catheter, Northern Digital, Canada) measures the voltage induced in the AC magnetic fields to estimate the gradient of the magnetic field strength. After being increased by the pre-amplifier (LT1167a, Linear Technology, USA), the measured voltage is acquired by the analog to digital converter (ADC) and sent back to the PC inside the system chassis (PXIe-1078, National Instrument, USA). The PC processes the measured signals, estimates the 5DOF tracker pose and controls the entire system.

Ramp waveform excitation

This work is based on modeling a conductive distorter as an additional resistance-inductance (RL) circuit [20]. For general AC EMTS, the frequencies of the generated signals are much lower than the self-resonant frequencies of the wires and coils. Therefore, the capacitive effects are insignificant in analyzing the inductive coupling between the coils. Figure 2 illustrates the equivalent circuit model of the inductive coupling of a transmitter coil and a sensor coil, with a nearby conductive distorter.

The generated voltage signal U_g is increased by the amplifier of the transmitter coil with a gain of A_T; after this amplification, the voltage U_T across the transmitter coil is increased to $A_T U_g$. The resistance of the circuit is R_T, and the inductance of the transmitter coil is L_T. The sensor coil circuit and the conductive distorter can also be modeled as RL circuits with the resistances R_S, R_D and inductances L_S, L_D, respectively. The voltage U_S across the sensor coil circuit due to the coil coupling, after being amplified, can be measured by the PXI system. The mutual inductance between the transmitter and sensor coil, distorter and transmitters/sensors is described as M_{T-S}, M_{T-D} and M_{S-D}.

The time constants of the transmitter coil and conductive distorter circuits are important for the circuit analysis and can be calculated as [21]:

$$\tau_T = \frac{L_T}{R_T} \tag{2}$$

$$\tau_D = \frac{L_D}{R_D} \tag{3}$$

The transfer function of the inductive coupling between the transmitter and the sensor was calculated as follows [22]:

$$G_{T-S} = \frac{U_S}{U_T} = \frac{s M_{T-S}}{L_T \left(\frac{1}{\tau_T} + s\right)} \tag{4}$$

Supplying a ramp waveform signal of $K \cdot t$ as the system input excitation, the voltage induced in the sensor coil can be calculated by (5) and (6), in Laplace and time domain.

$$U_{S-T}(S) = \frac{K M_{T-S}}{L_T \cdot s \left(s + \frac{1}{\tau_T}\right)} \tag{5}$$

$$U_{S-T}(t) = \frac{K M_{T-S} \tau_1 \left(1 - e^{-\frac{t}{\tau_T}}\right)}{L_T} \tag{6}$$

Here, the system response to a ramp excitation comprises two parts: a horizontal line and an exponential curve due to the switch-on cycle. The Laplace transfer functions of the inductive couplings between L_T and L_D, L_D and L_S are illustrated by (7) and (8).

$$G_{T-D} = \frac{s M_{T-D}}{L_T \left(s + \frac{1}{\tau_T}\right)} \tag{7}$$

$$G_{D-S} = \frac{s M_{S-D}}{L_D \left(s + \frac{1}{\tau_D}\right)} \tag{8}$$

The voltage across the sensor coil due to the magnetic field generated by the conductive distorter can be calculated in the Laplace and time domain.

$$U_{S-D}(S) = \frac{K M_{T-D} M_{S-D}}{L_T \cdot L_D \cdot \left(s + \frac{1}{\tau_T}\right)\left(s + \frac{1}{\tau_D}\right)} \qquad (9)$$

$$U_{S-D}(t) = \frac{K M_{T-D} M_{S-D} \tau_T \tau_D \left(-e^{-\frac{t}{\tau_D}} + e^{-\frac{t}{\tau_T}}\right)}{L_T \cdot L_D (\tau_T - \tau_D)} \qquad (10)$$

The total voltage comprises distorted and non-distorted information is shown in (11).

$$U_S(t) = \frac{K M_{T-S} \tau_T \left(1 - e^{-\frac{t}{\tau_T}}\right)}{L_T}$$
$$+ \frac{K M_{T-D} M_{S-D} \tau_T \tau_D \left(-e^{-\frac{t}{\tau_D}} + e^{-\frac{t}{\tau_T}}\right)}{L_T \cdot L_D (\tau_T - \tau_D)} \qquad (11)$$

The non-distorted voltage comprises a horizontal line element of $\frac{K M_{T-S} \tau_T}{L_T}$ and an exponential element of $-\frac{K M_{T-S} \tau_T e^{-\frac{t}{\tau_T}}}{L_T}$, while the distorted voltage only contains exponential parts. As seen in (11), the larger the time variable t we choose, the exponential components of $e^{-\frac{t}{\tau_T}}$ and $-e^{-\frac{t}{\tau_D}}$ approach more to 0. In reality, t must not be any large number to avoid low refresh time and bad SNR.

Simulation

In our experimental setup, $L_T = 1.2\,\text{mH}$, $R_T = 15\,\Omega$, $\tau_T = \frac{L_T}{R_T} = 0.08\,\text{ms}$. We assumed the metal distorter as a common material for the medical instrument: aluminum. The resistivity of aluminum at $20\,^\circ\text{C}$ is $2.65 \times 10^{-8}\,\Omega\,\text{m}$. It is assumed to be a regular shaped cylinder with a length of 100 mm and a diameter of 10 mm. Equation 12 shows the calculation of the resistance $-\rho, l, A$ representing the resistivity, length and cross-sectional area. The resistance of such a distorter model was calculated to be $3.4 \times 10^{-5}\,\Omega$.

$$R_D = \rho \frac{l}{A} \qquad (12)$$

The self-inductance of the aluminum distorter is calculated to be $6.0 \times 10^{-8}\,H$, using Eq. 13 [23]:

$$L_D = 0.002\left[\ln\left(\frac{2l}{r}\right) - \frac{3}{4})\right]\,\text{mH} \qquad (13)$$

where r is the radius of the cylinder conductor. The time constant of the conductor in this example was calculated to be 1.8 ms. The self-inductance of the distorter can be estimated by the known magnetic flux and the current flow in the distorter. The mutual inductances between the transmitter coil, sensor coil, and conductive distorter are calculated using (14)–(16).
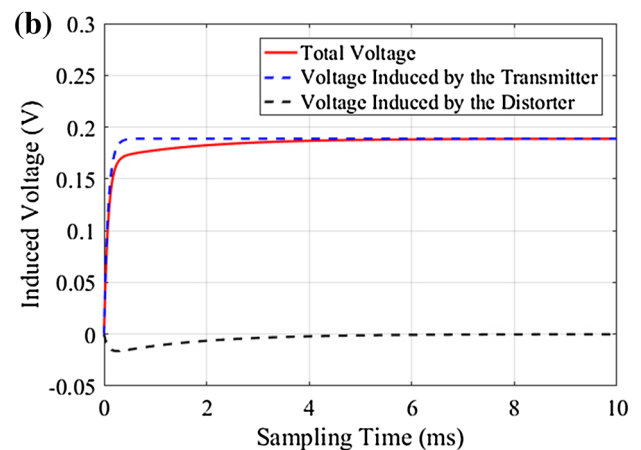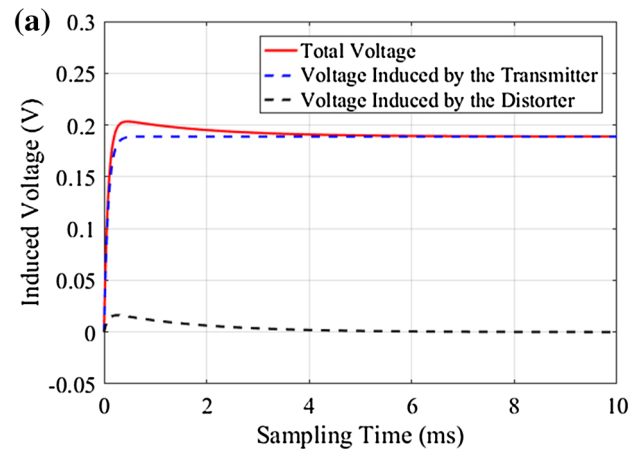
Fig. 3 An example of the simulated voltage measurement with a conductive distorter nearby the sensor coil: **a** additive conductive distortion, **b** subtractive conductive distortion between sensor and distorter

$$M_{T-S} = k_{T-S} \cdot \sqrt{L_T L_S} \qquad (14)$$
$$M_{T-D} = k_{T-D} \cdot \sqrt{L_T L_D} \qquad (15)$$
$$M_{S-D} = k_{S-D} \cdot \sqrt{L_S L_D} \qquad (16)$$

where k_{T-S}, k_{T-D} and k_{S-D} are the coupling coefficients between air coils which are typically smaller than 0.35 [24]. When the distance between the coils grows larger, the coupling coefficient becomes smaller. The change in the coupling coefficient only changes the amplitude of the voltage signals, which does not influence the time constant of the distorter. We assume that the air coupling coefficients are standard, all being equal to 0.1. The conductive distortions can be additive or subtractive according to positive or negative directions of the current flows across the metallic distorter, relative to current flows in the sensor coil.

As the simulation result is shown in Fig. 3, the red curves represent the voltage signal induced in the sensor coil includ-
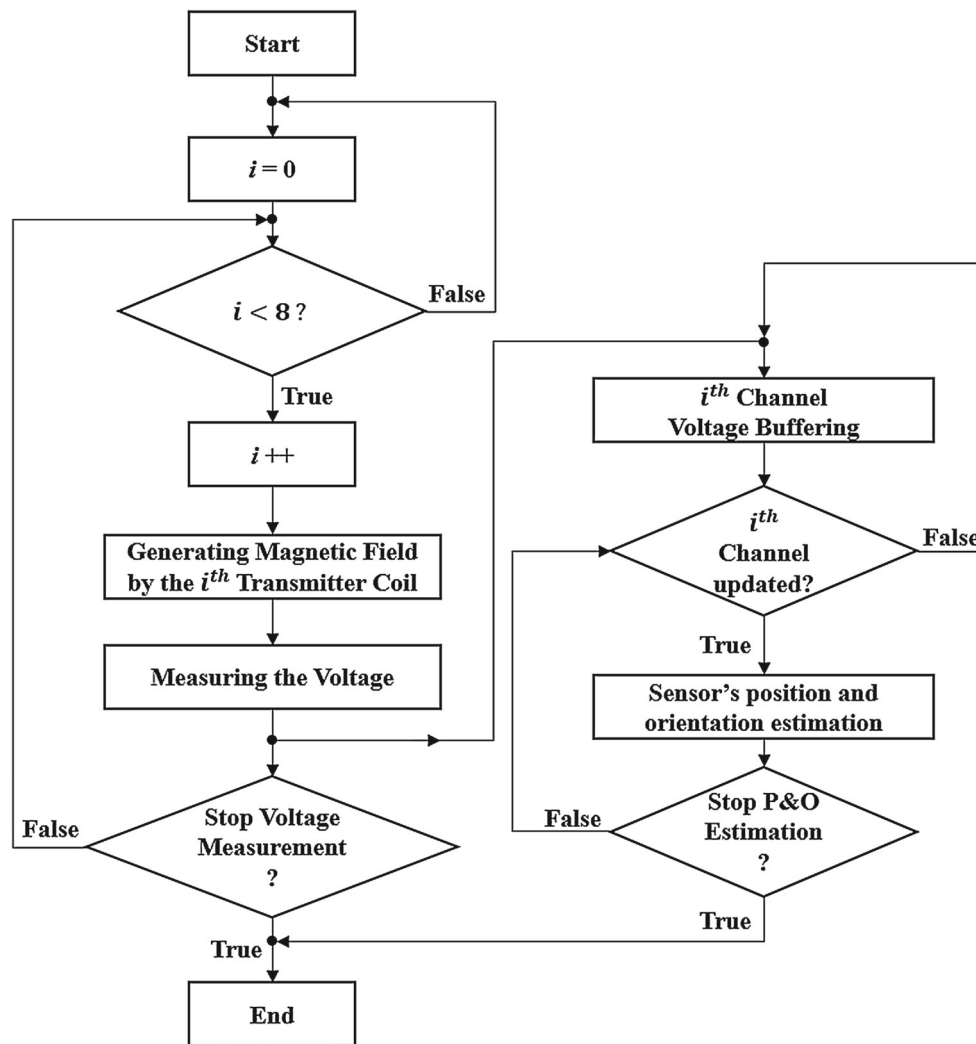
Fig. 4 The system block diagram of the fast data acquisition method

ing the information of the reference voltage signal induced by the transmitter coil (blue-dash) and the distorted signal caused by a conductive object (black-dash). In realities, only the voltage induced in the sensor coil is measured. Because of the switch-on cycle effect, a delay of $5 \times \tau_T = 0.4$ ms was added for the system response approximately reaching its steady state. In this example, the "Total voltage" between 9.4 and 10 ms is approximately equal to the non-distorted voltage.

Data acquisition

The direct digital synthesis (DDS) technology is used to generate eight channel ramp waveforms. Time division multiplexing (TDM) is a standard method for sensor pose estimation; the signals were generated and measured sequentially from the first to the last channel in continuous time with

one update in sensor's pose. In this work, a fast TDM method was developed as shown in Fig. 4.

Within this approach, the DAQ and pose estimation are running in parallel loops. The measured voltages induced by different transmitter coils are buffered in the system memory. It is a moving-average-like acquisition process wherein the other channels remain in the last state when the ith channel is updated. To realize this, eight on-board FPGA target-to-target FIFOs were used to individually acquire the signals in the eight channels. Additionally, an FPGA target-to-host FIFO was utilized to acquire the data measured by the eight FPGA target-to-target FIFOs and transfer it to the PC using direct memory access (DMA). For each channel, five periods of the signals were measured.

Figure 5 shows an example of generated and measured voltage signals of the DAQ device. In our current approach, five steps' averaging is necessary to improve the signal quality.

Fig. 5 Generated and measured voltages: **a** voltage generated by DAC and **b** an example of the voltage induced by one of the eight transmitter coils measured by ADC
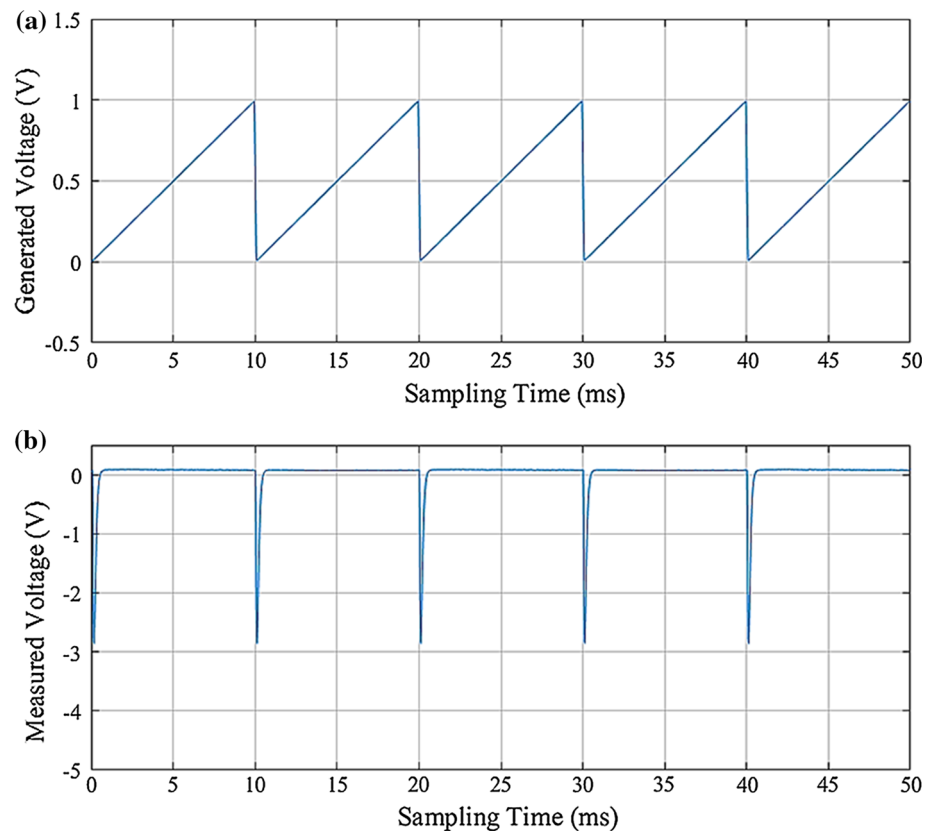
Pose estimation

The algorithm for pose estimation using dipole approximation referred in the literature [25]. By minimizing the differences between the measured and the estimated voltages across the sensor coil, the actual sensor pose can be estimated as is shown in (17).

$$F(x, y, z, \theta, \varphi) = \sum_{i=1}^{n} \left(\left| U_{\text{mea}}^{i} - U_{\text{est}}^{i} \right| \right) \quad (17)$$

For the ramp waveform excitation method introduced in this paper, U_{mea} is equal to the horizontal linear signal $\frac{K M_{\text{T}-\text{S}} \tau_{\text{T}}}{L_{\text{T}}}$ in (11).

Evaluation

Refresh rate

System refresh rate by using the ramp, QR, and sinusoidal excitation was evaluated individually.

As shown in Fig. 6, the catheter was previously inserted in the vascular phantom at a fixed position (2). A medical catheter pullback device was utilized to pull out the catheter from the vascular phantom at a constant speed of
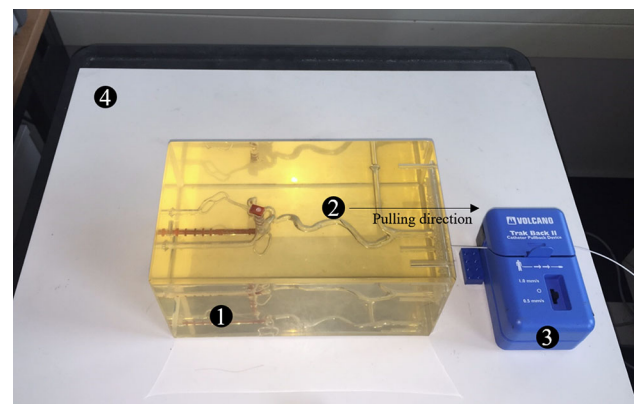

Fig. 6 System refresh rate measurement: *1* vascular phantom, *2* the tip of the catheter, *3* catheter pullback device (Trak Back II, Volcano, Japan) and *4* field generator

0.5 mm/s over 100 s. The total frames of the sensor's pose were recorded to calculate the system refresh rate.

Time constant measurement

The time constant of the transmitter coil τ_{T} is a fixed value in our experimental setup. However, for the conductive distorter, τ_{D} is changeable due to different size and materials of
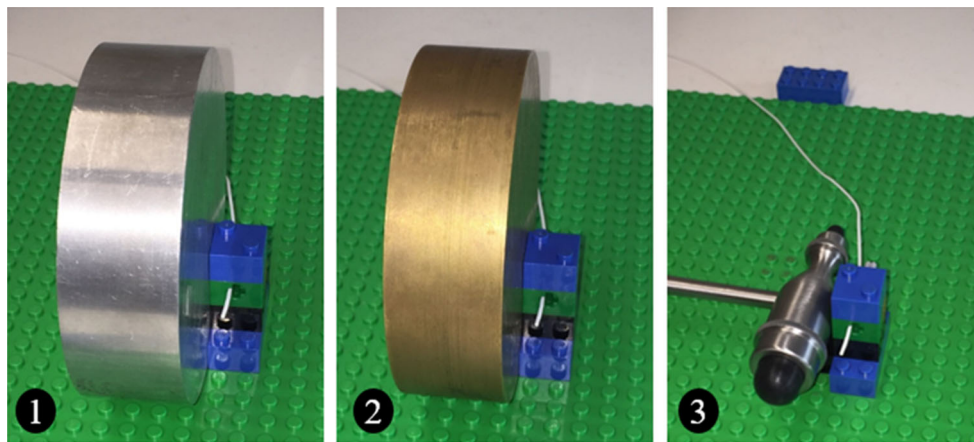
Fig. 7 Time constant measurement of metal distorters: *1* an aluminum disk with a diameter of 10 cm and thickness of 3 cm, *2* a brass disk with a diameter of 10 cm and thickness of 3 cm, *3* a neurological reflex hammer

the metallic objects. Figure 7 shows the measurement of the time constants of different metallic distorters.

In this measurement, the sensor coil was fixed on the top of the field generator. The conductive distorters were individually placed approximately 0.5 cm close to the sensor coil. A unit step waveform was generated and supplied to the first of the transmitter coil. The system response to the unit step excitation was measured to calculate the time constant of the three conductive distorters (Fig. 8).

Positional accuracy

The assessment of the static tracker accuracy using the ramp excitation method was performed by using an optical tracking system—NDI Polaris Spectra (*Northern Digital, Canada*) as the reference positioning system.

In this measurement, the EM sensor was moved by the LEGO robot in the wooden test volume along X, Y, Z directions automatically. 512 poses were measured by the EMTS and OTS, respectively. The pose measured by the optical tracking system can be utilized as a reference to calculate the EMTS sensor error (18) and (19):

$$E_P(i) = \sqrt{\left(X_{op}(i) - X_{em}(i)\right)^2 + \left(Y_{op}(i) - Y_{em}(i)\right)^2 + \left(Z_{op}(i) - Z_{em}(i)\right)^2}$$

$$(18)$$

$$E_O(i) = \sqrt{\left(\varphi_{op}(i) - \varphi_{em}(i)\right)^2 + \left(\theta_{op}(i) - \theta_{em}(i)\right)^2} \quad (19)$$

Here, *i* represents the *i*-th of the total 512 poses. *E* is the total position error of the EM sensor. X_{op}, Y_{op}, Z_{op}, φ_{op} and θ_{op} are the measured marker pose by OTS used as the reference positions. Meanwhile, X_{em}, Y_{em}, Z_{em}, ϕ_{em} and θ_{em} are the measured sensor pose by EMTS. The mean error (ME) and root-mean-square error (RMSE) were calculated using (20) and (21).
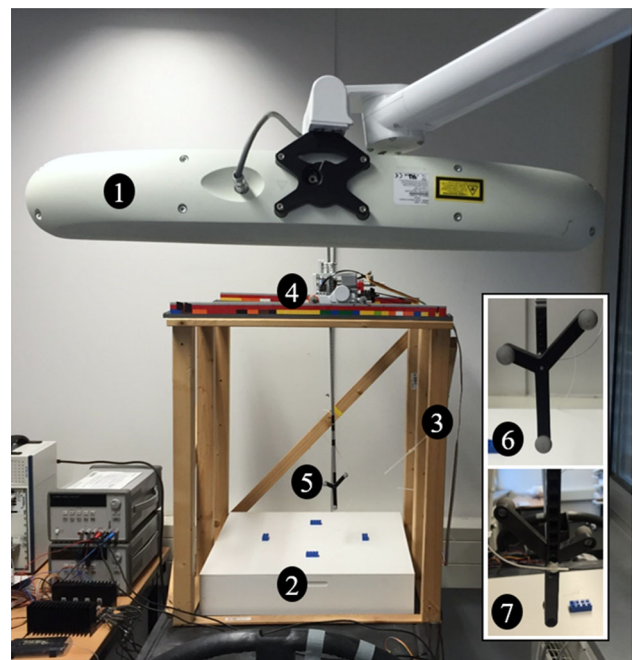

Fig. 8 Sensor pose accuracy assessment: *1* optical tracking system, *2* EM field generator, *3* test volume defined by a wooden structure, *4* LEGO robot being used to move the tracker in the 3D test volume, *5* optical marker/EM sensor with fixed locations: *6* front view—optical markers, *7* back view—rigidly fixed EM sensor

$$ME = \frac{1}{n} \sum_{i=1}^{n} E(i) \quad (20)$$

$$RMSE = \sqrt{\frac{\sum_{i=1}^{n} E(i)^2}{n}} \quad (21)$$

Due to the limitation of established LEGO frame, the sensor coil was fixed toward one direction. Therefore, the
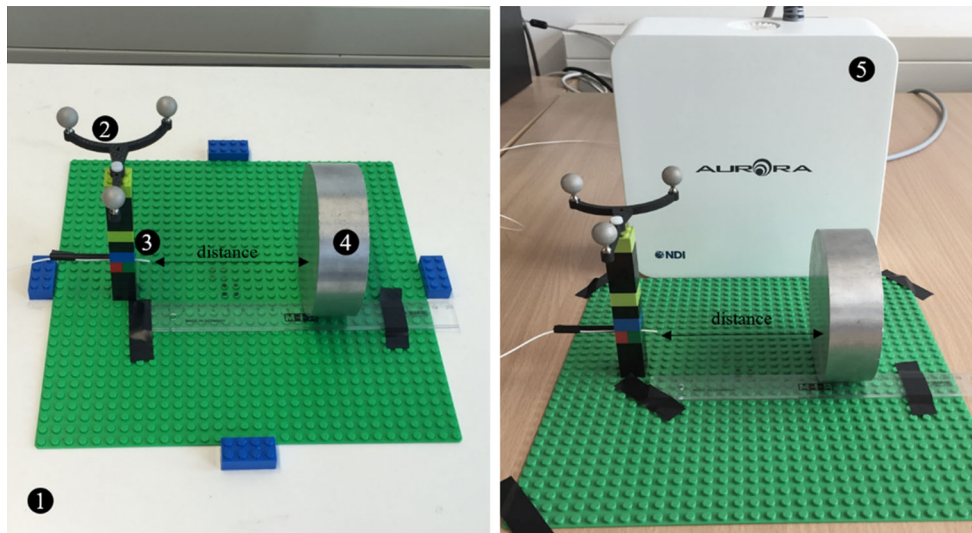
Fig. 9 Measurement of sensor pose error due to a nearby conductive distorter at different distance from 10 to 1 cm to the sensor coil: *1* field generator of the experimental setup, *2* optical marker with fixed pose to the sensor coil, *3* sensor coil, *4* conductive distorter, and *5* field generator of NDI Aurora system

accuracy of sensor coils' orientation was not comprehensively evaluated by this setup.

Distance-dependent distortion

To estimate the sensor pose error due to the changes in the distance between the sensor coils and the conductive distorters, we performed a measurement as illustrated in Fig. 9.

Here, aluminum/ brass disks and a reflex hammer, shown in Fig. 4, were tested. The metal objects were placed 10 cm away and moved toward the sensor coil, to a distance of 1 cm from the coil. In this measurement, the optical tracking system was utilized to provide the basis of the original sensor's location. The changes in sensor's poses measured by EMTS, due to distorters placed at various distances, were compared. The measurements were performed applying sinusoidal/ ramp excitations and also on a commercial ETMS. In order to minimize the influence of noise on the tracked sensor's poses, each measurement was repeated 1000 times for averaging.

Distortions from medical instruments

We tested the system performance against distortions from a brass disk of different size, multiple clinical instruments, and devices. Figure 10 shows the different sources of metallic distortions for EMTS. In this experiment, the different sources of distortions were all fixed 1 cm away to the sensor coil on our setup and also the commercial EMTS.

Fig. 10 Sources of distortions: *1* 5 cm × 1 cm brass disk, *2* dental drill body, *3* Langenbeck hook, *4* bone curettes, *5* scalpel, *6* needle holder, *7* ultrasound probe

Results

Refresh rate

The system refresh rate was measured to be 12.7 fps. Table 1 shows the comparisons of the system refresh rate among the different methods running on our experimental setup.

Time constant measurement

The time constant of an aluminum disk, a brass disk and a neurological reflex hammer as seen in Fig. 6 was measured and is presented in Fig. 11.

The voltage induced in the sensor coil was measured and shown in Fig. 10. The measured voltages between 2.58 and

Table 1 System refresh rate of our experimental setup

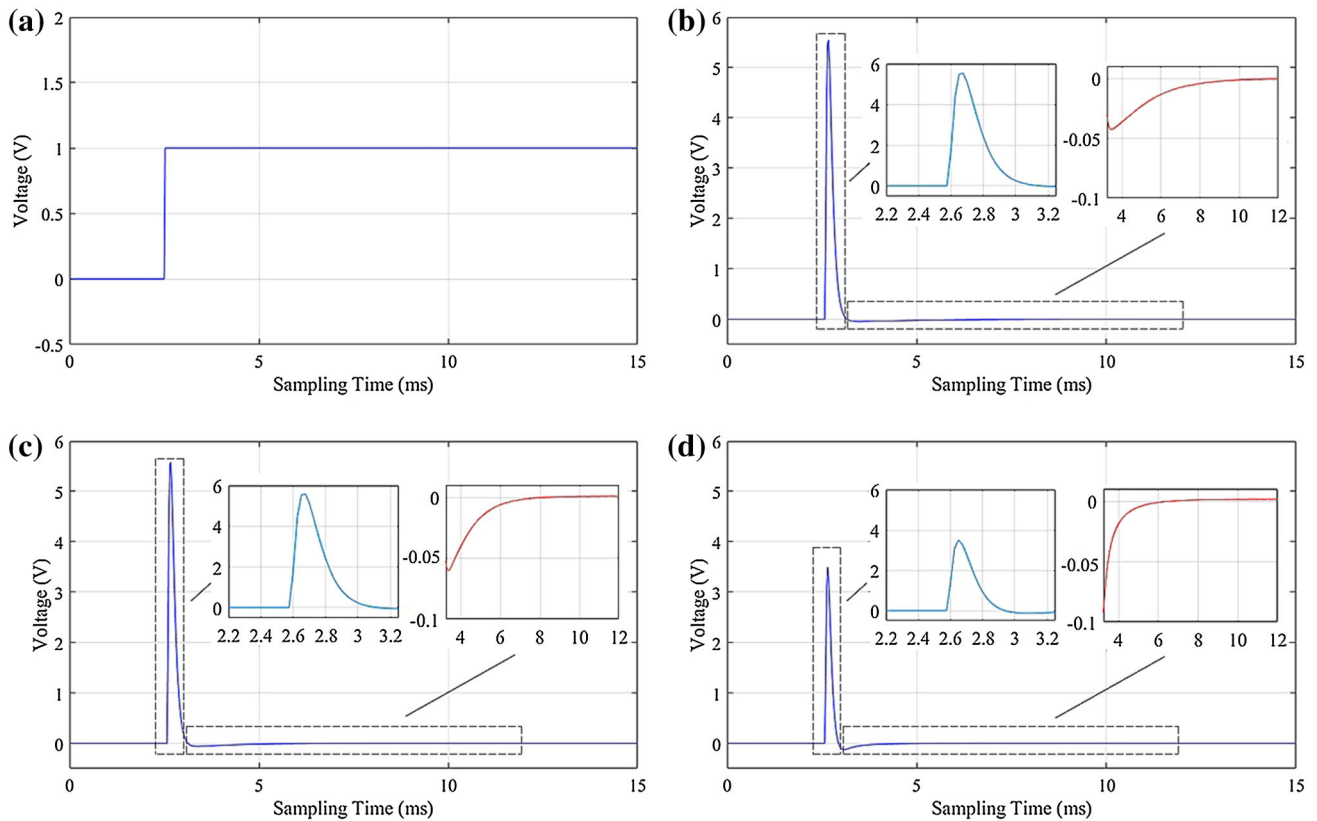| Method	Sine-TDM [26]	Sine-FDM [26]	QR-TDM [19]	Ramp-fast TDM
Refresh rate (fps)	6.3	34.4	1.5	12.7

Fig. 11 The measured voltage due to a unit step excitation for distinct conductive distortions: **a** unit step excitation, **b** system response to an aluminum disk, **c** system response to a brass disk, and **d** system response to a neurological reflex hammer

3.2 ms provide information about the system switch-on cycle, the time constant of transmitter coils and the time constant of conductive distorters. The measured voltage between 3 and 15 ms only shows the decay of the voltage stored in the conductive distorters. The time constant of the aluminum disk, brass disk, and a reflex hammer was measured to be 1.72, 0.98, and 0.75 ms, respectively.

Conductive distorters with different shapes and materials have corresponding distinct time constants. As is shown in Fig. 6, the aluminum disk has the biggest time constant. Here, the system needs at least $1.72 \times 5 + 0.62 = 9.22$ ms to approximately reach its steady state. For the proximate brass disk and reflex hammer, the system needs 5.52 ms and 4.37 ms to reach its steady state.

Positional accuracy

Figure 12 and Table 2 present the results of the sensor pose corresponding to the distinct distances between the sensor and the transmitter coils.
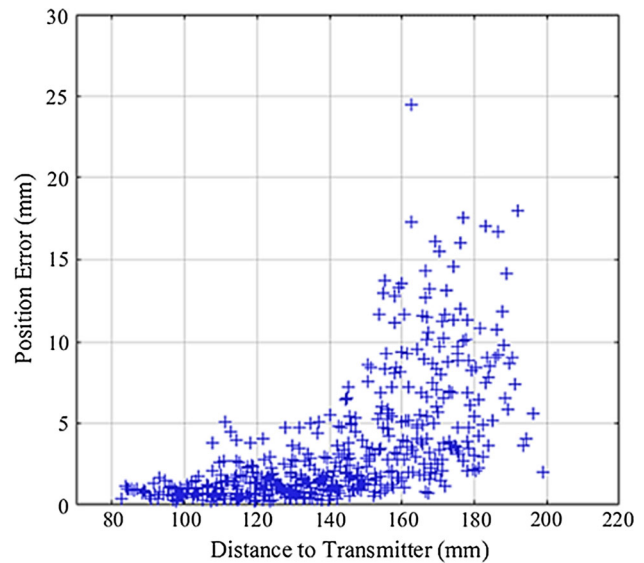

Fig. 12 Sensor position error in the test volume with distance between the sensor and the center of the transmitter coils array of up to 200 mm

Table 2 Sensor position error varies with different distances between the sensor and the center of the transmitter coil array

Distance	100 mm	150 mm	200 mm
Position error (mm)			
Mean	0.70	1.28	3.41
RMS	0.77	1.55	5.11
Max	1.75	5.42	25.28

Distance-dependent distortion

The measurement—as shown in Fig. 8—aiming to analyze the level of errors in estimated sensor's pose due to the different distances between the sensor and transmitter was taken. The result is shown in Fig. 13.

The errors of estimated sensor's poses increase when the distances between the sensor and the distorter decrease, for the NDI Aurora system and our experimental setup applying

sinusoidal excitation. Missing measurement occurred for the NDI Aurora system when the aluminum and brass disks were placed 1 cm away from the sensor coil. The ramp excitation method reduces the errors of the estimated sensor's pose due to aluminum and brass disks at distances lower than 0.5 mm in position and 0.8° in orientation. However, it cannot reduce the errors caused by the reflex hammer made of stainless steel to such a low level.

Distortions from medical instruments

Sensor pose error for both the commercial system and our EMTS prototype using sinusoidal and ramp excitation caused by distinct instruments is presented in Fig. 14.

The largest sensor pose errors for the commercial ETMS and sinusoidal excitation are 4.93, 5.30 mm in the estimated position, caused by the brass disk, and 6.23°, 4.22° in orientation, caused by the needle holder. Our setup applying ramp excitation reduces sensor pose error caused by the different
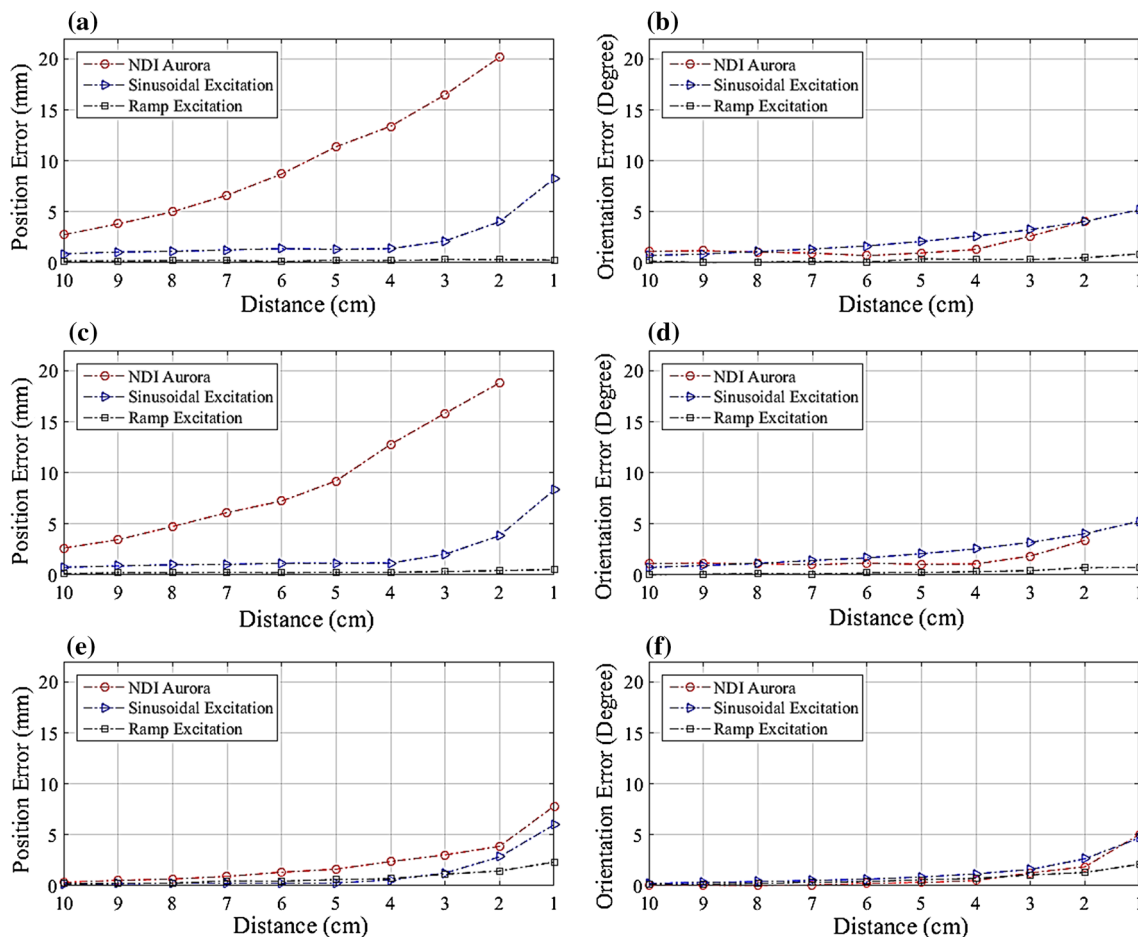

Fig. 13 Sensor pose error due to conductive distorters placed at different distances to the sensor coil: **a** position error due to an aluminum disk, **b** orientation error due to an aluminum disk, **c** position error due to a brass disk, **d** orientation error due to a brass disk, **e** position error due to a reflex hammer, and **e** orientation error due to a reflex hammer
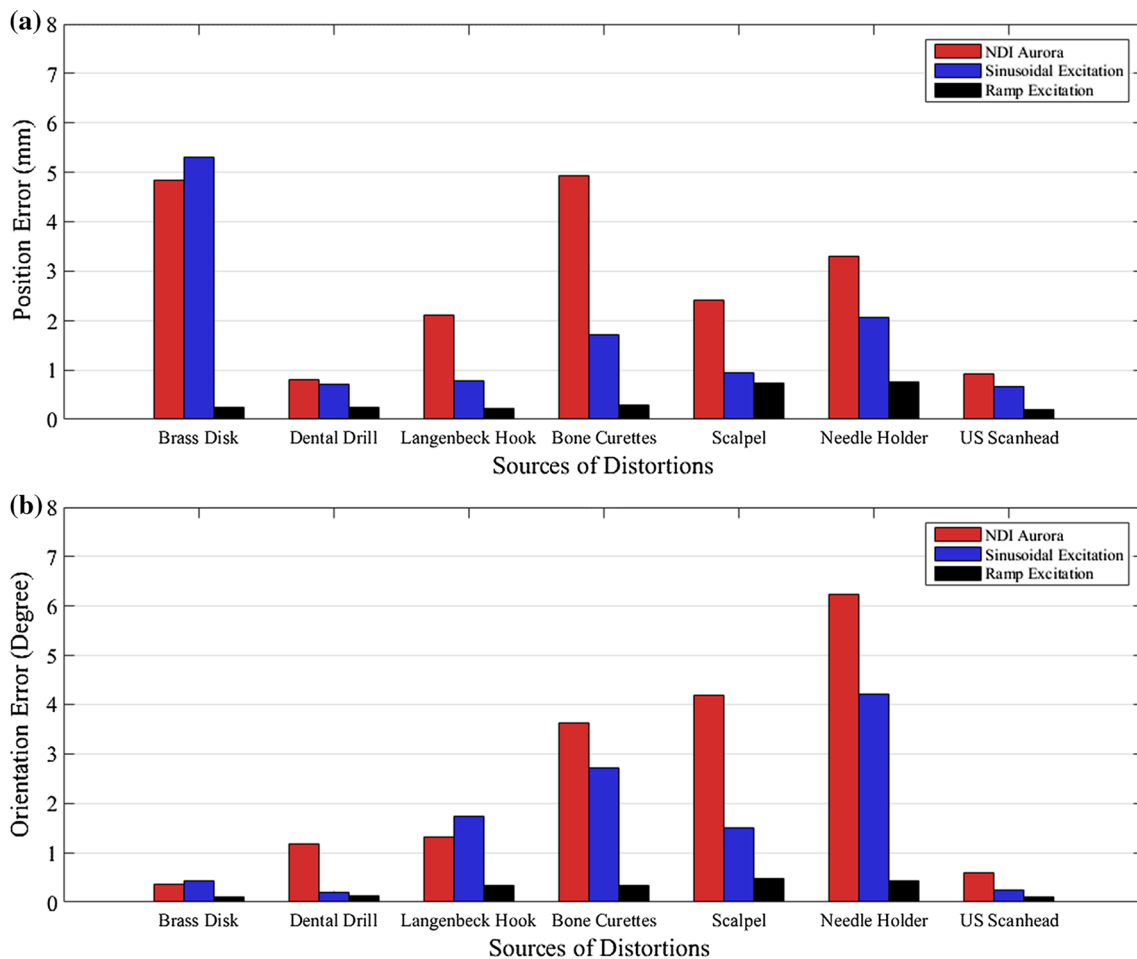
Fig. 14 Sensor pose's error resulting from different sources of distortion for our experimental setup applying ramp/ sinusoidal excitations and the commercial system: **a** sensor position error, **b** sensor orientation error

distorters with the maximum position error of 0.75 mm and 0.48°.

Discussion

Refresh rate

Given the Fast TDM method and the implementation using an FPGA, the system features a refresh rate of 12.7 Hz. The ramp method is slower than the sinusoidal excitation method applying FDM due to a much lower input signal frequency. The FDM method does not support the ramp excitation method because the system response in the time domain cannot be filtered out by band-pass filters.

Latency

In this work, five periods of the measured voltage signals were averaged to increase the signal quality. As shown in

Fig. 5, for a complete estimation of sensor's pose, the system needs 50×8 ms $= 400$ ms to measure the voltages induced in all channels. The computational process also consumes some time. Therefore, our current approach has a delay of approximately 431 ms to completely estimate the sensor's pose.

Tracker accuracy

Regarding the tracker accuracy, the expected error is less than 2 mm. Our approach meets this requirement when the distance between the sensor and the center of the transmitter coils is less than 150 mm. The tracker pose error is greater when the distance increases, because of a poorer SNR of the measured system response to the ramp excitation. In the current setup, the arrangement of the transmitter coils' position and orientation were randomly predefined. Optimization of the transmitter coils' position and orientation can be performed to let higher magnetic flux pass through the cross-sectional area of the sensor coil to measure larger

voltage drops. This will lead to a better SNR in the measured voltage induced in the sensor coil, allowing the system to attain a higher precision in the sensor's pose estimation. The hardware of the system can be optimized to increase the SNR further. Application of sophisticated filters such as the Kalman filter, which have the potential to improve the robustness as well as speed up the frame rate, can be investigated. These improvements may enhance the accuracy and robustness of the ramp excitation method for EMTS in a much larger working volume.

Metallic distortions

A comparison with a commercial system and the sinusoidal excitation method in the presence of proximate conductive distorters was performed. The commercial EMTS and our setup applying sinusoidal excitation demonstrated significant errors due to a proximate conductive distorter. The system utilizing ramp excitations reduced such errors to a very low level. The ramp excitation method reduces the pose errors caused by pure non-ferromagnetic materials, such as aluminum and brass disks, to a significantly low level. However, there was still an obvious error when certain medical instruments made of stainless steel, such as a reflex hammer or a needle holder, were located close to the sensor coil. Although austenitic stainless steel is non-ferromagnetic, other types of stainless steels such as ferritic, martensitic and duplex are ferromagnetic. Our approach reduces the errors caused by conductive but non-ferromagnetic materials.

Comparison with commercial systems

Our current approach on the EMTS prototype is slower in updating sensor's pose signals compared to the commercial EMTS, which generally provides refresh rates between 40 and 250 Hz [7]. The latency of the Ascension *Flock of Birds* and the Polhemus *Fastrak* system was measured to be approximately up to 50 ms [27], which is much lower than our approach in removing conductive distortions. With respect to spatial positioning accuracy, NDI's *Aurora* system was reported to have a position RMS error of 1.2 mm with the distance between the sensor and field transmitter up to 600 mm, evaluated by using an optical tracking system [28]. The accuracy of our current approach is 1.6 mm RMS error within a distance of up to 150 mm. The main advantage of our approach is the improved robustness against proximate conductive distorters. In fact, as illustrated in Figs. 13 and 14, our method provides a significantly better performance on the robustness against distorters than the commercial system.

Future work

This paper introduces a software-based solution to reduce tracking errors caused by electrically conductive objects in operating rooms. Before putting it forward into the use of real clinical applications, the system needs to be further improved and more comprehensively evaluated. In this work, we have assessed the tracking accuracy utilizing an optical tracking system as the reference positioning system. As documented by its manufacturer, the NDI *Polaris Spectra* has a 0.25 mm RMS error. Due to the error distributions of this system as was reported in [29], we carefully selected the testing volume. However, the positions measured by this optical tracking system do not provide the ground truth with sufficient precision. The results in Fig. 12 and Table 2 show the error distributions and its potential for use in clinical applications. In future work, more accurate optical tracking systems such as the Atracsys *fusionTrack 500* or laser-based tracking systems such as the FARO *Laser Tracker*, with much higher accuracies, have to be applied as reference positioning systems. With respect to statistically evaluating the orientation accuracy, test phantoms having very small error tolerances and setups allowing the changing of the sensor's orientations [30] have to be applied.

The current approach of this method has a delay of up to 431 ms in updating the sensor's pose. In order to reduce the delay in the future, one solution is an adaptive truncation of the ramp-signal periods. In this work, we chose a measurement time of 10 ms for each excitation. It allows the distortions caused by conductive materials, whose conductivities are smaller than aluminum, to be removed. In the future, an adaptive process for choosing the optimal time with regard to different levels of distortions will be investigated. From small to large conductive distortions, the system will automatically choose the most suitable periods of the ramp input signals. A very weak point of our basic prototype is the hardware, which has not been optimized with respect to electronic noise, the amplifier of the test coil, or the transmitter coils' arrangement. These aspects have to be improved in the future. Furthermore, sophisticated filters, e.g. Kalman filter, will be applied in order to shorten the averaging periods and increase the tracking accuracy. It should also be noted that all calculations are done with MATLAB, causing avoidable delays. Last but not least, the current implementation focusses on reducing metallic distortions. However, when there is no metal object proximate to the sensor coil, the standard method using sine-wave excitation lets the system to operate more accurately in a larger working volume and with much faster measurement speed. Therefore, a more intelligent solution would be adaptive switching between sinusoidal and ramp excitation methods for EMTS, after detecting whether or not there is a proximate conductive distorter.

Conclusion

This work represents a proof of the concepts for a method based on ramp waveform excitation which can strongly reduce the distortions of EMTS caused by proximate metallic conductors. This purely software-based procedure currently provides a low refresh rate of 12.7 fps and a relatively small volume of interest for precise tracking. However, since the reasons for these issues are well understood, the implementation can be straightforwardly improved.

Compliance with ethical standards

Conflict of interest Mengfei Li, Christian Hansen and Georg Rose declare that they have no conflict of interest.

References

1. Wood BJ, Zhang H, Durrani A, Glossop N, Ranjan S, Lindisch D, Levy E, Banovac F, Borgert J, Krueger S, Kruecker J, Viswanathan A, Cleary K (2005) Navigation with electromagnetic tracking for interventional radiology procedures: a feasibility study. J Vasc Interv Radiol 16:493–505. doi:10.1097/01.RVI.0000148827.62296.B4
2. Shahriari N, Hekman E, Oudkerk M, Misra S (2015) Design and evaluation of a computed tomography (CT)-compatible needle insertion device using an electromagnetic tracking system and CT images. Int J Comput Assist Radiol Surg 10:1845–1852. doi:10.1007/s11548-015-1176-3
3. Sorger H, Hofstad EF, Amundsen T, Langø T, Leira HO (2016) A novel platform for electromagnetic navigated ultrasound bronchoscopy (EBUS). Int J Comput Assist Radiol Surg 11:1431–1443. doi:10.1007/s11548-015-1326-7
4. Watzinger F, Birkfellner W, Wanschitz F, Millesi W, Schopper C, Sinko K, Huber K, Bergmann H, Ewers R (1999) Positioning of dental implants using computer-aided navigation and an optical tracking system: case report and presentation of a new method. J Craniomaxillofac Surg 27:77–81
5. Boutaleb S, Racine E, Fillion O, Bonillas A, Hautvast G, Binnekamp D, Beaulieu L (2015) Performance and suitability assessment of a real-time 3D electromagnetic needle tracking system for interstitial brachytherapy. J Contemp Brachytherapy 7:280–289. doi:10.5114/jcb.2015.54062
6. Birkfellner W, Watzinger F, Wanschitz F, Enislidis G, Kollmann C, Rafolt D, Nowotny R, Ewers R, Bergmann H (1998) Systematic distortions in magnetic position digitizers. Med Phys 25:2242. doi:10.1118/1.598425
7. Nafis C, Jensen V, Beauregard L, Anderson P (2006) Method for estimating dynamic EM tracking accuracy of surgical navigation tools. In: Cleary KR, Galloway Jr. RL (eds) Medical imaging, vol 6141, pp 152–167. doi:10.1117/12.653448
8. Kuchel PW, Chapman BE, Bubb WA, Hansen PE, Durrant CJ, Hertzberg MP (2003) Magnetic susceptibility: solutions, emulsions, and cells. Concepts Magn Reson 18A:56–71. doi:10.1002/cmr.a.10066
9. Garikepati P, Chang TT, Jiles DC (1988) Theory of ferromagnetic hysteresis: evaluation of stress from hysteresis curves. IEEE Trans Magn 24:2922–2924. doi:10.1109/20.92289
10. Poulin F, Amiot L-PL-P (2002) Interference during the use of an electromagnetic tracking system under OR conditions. J Biomech 35:733–7. doi:10.1016/S0021-9290(02)00036-2
11. Kindratenko VV (2000) A survey of electromagnetic position tracker calibration techniques. Virtual Real 5:169–182. doi:10.1007/BF01409422
12. Plotkin A, Kucher V, Horen Y, Paperno E (2008) A new calibration procedure for magnetic tracking systems. IEEE Trans Magn 44:4525–4528. doi:10.1109/TMAG.2008.2003056
13. Dumoulin CL (2001) Error compensation for device tracking systems employing electromagnetic fields. Patent US 6,201,987
14. Jascob B, Kessman P, Simon D, Smith A (2003) Method and apparatus for electromagnetic navigation of a surgical probe near a metal object. Patent US 6,636,757
15. Rolland JP, Larry DD, Bailot Y (2001) A survey of tracking technology for virtual environments. In: Barfield W, Caudell T (eds) Fundamentals of wearable computers and augmented reality. CRC Press, New Jersey, p 836
16. Anderson PT (2010) Ultra-low frequency electromagnetic tracking system. Patent US 7,761,100
17. Hansen PK, Ashe WS (1998) Magnetic field position and orientation measurement system with dynamic eddy current rejection. Patent US 5,767,669
18. Paperno E, Sasada I, Leonovich E (2001) A new method for magnetic position and orientation tracking. IEEE Trans Magn 37:1938–1940. doi:10.1109/20.951014
19. Bien T, Li M, Salah Z, Rose G (2014) Electromagnetic tracking system with reduced distortion using quadratic excitation. Int J Comput Assist Radiol Surg 9:323–32. doi:10.1007/s11548-013-0925-4
20. Nieminen JM, Kirsch SR (2010) Eddy current detection and compensation. Patent US 7,783,441
21. Hajimiri A (2010) Generalized Time- and Transfer-Constant Circuit Analysis. IEEE Trans Circuits Syst I Regul Pap 57:1105–1121. doi:10.1109/TCSI.2009.2030092
22. Doetsch G (1974) Introduction to the theory and application of the Laplace transformation. doi:10.1007/978-3-642-65690-3
23. Rosa EB (1908) The self and mutual inductances of linear conductors. In: Bulletin Bureau Stand. U.S. Dept. of Commerce and Labor, Bureau of Standards, pp 302–305
24. Meade RL (2002) Foundations of electronics. Cengage Learning, Boston, USA
25. Raab F, Blood E, Steiner T, Jones H (1979) Magnetic position and orientation tracking system. IEEE Trans Aerosp Electron Syst AES 15:709–718. doi:10.1109/TAES.1979.308860
26. Li M, Bien T, Rose G (2013) FPGA based electromagnetic tracking system for fast catheter navigation. Int J Sci Eng Res 4:2566–2570. doi:10.14299/ijser.2013.09.001
27. Adelstein BD, Johnston ER, Ellis SR (1996) Dynamic response of electromagnetic spatial displacement trackers, vol 5, no 3. Presence, Cambridge
28. Frantz DD, Wiles AD, Leis SE, Kirsch SR (2003) Accuracy assessment protocols for electromagnetic tracking systems. Phys Med Biol 48(14):2241–2251
29. Wiles AD, Thompson DG, Frantz DD (2004) Accuracy assessment and interpretation for optical tracking systems. In: Galloway Jr RL (ed) SPIE medical international society for optics and photonics, imaging, pp 421–432
30. Hummel J, Figl M, Birkfellner W, Bax MR, Shahidi R, Maurer CR, Bergmann H (2006) Evaluation of a new electromagnetic tracking system using a standardized assessment protocol. Phys Med Biol 51:N205-10. doi:10.1088/0031-9155/51/10/N01